Journal Name

ARTICLE

Cite this: DOI: 10.1039/x0xx00000x

Received ooth January 2012,
Accepted ooth January 2012

DOI: 10.1039/x0xx00000x

Conjugatable Water-Soluble Pt (II) and Pd(II) Porphyrin Complexes: Novel Nano- and Molecular Probes for Optical Oxygen Tension Measurement in Tissue Engineering

F. Giuntini,[a†] V. M. Chauhan,[b] J. W. Aylott,[b] G. A. Rosser,[c] A. Athanasiadis, [d] A. Beeby,[c] A. J. MacRobert, [d] R. A. Brown[d] and R. W. Boyle*[a]

Measurement of oxygen tension in compressed collagen sheets was performed using matrix-embedded optical oxygen sensors based on platinum(II) and palladium(II) porphyrins supported on polyacrylamide nanoparticles. Bespoke, fully water-soluble, monofunctionalised Pt(II) and Pd(II) porphyrin complexes designed for conjugation under mild conditions were obtained using microwave-assisted metallation. The new sensors display a linear response ($1/\tau$ *vs.* O_2) to varying oxygen tension over a biologically relevant range (7.0×10^{-4} to 2.7×10^{-1} mM) in aqueous solutions; a behaviour that is maintained following conjugation to polyacrylamide nanoparticles, and following embedding of the nanosensors in compressed collagen sheets, paving the way to innovative approaches for real-time resolution of oxygen gradients throughout 3D matrices useful for tissue regeneration.

Introduction

In the recent years, interest in the development of novel porphyrins for biomedical applications grew beyond the boundaries of the therapeutic field. An increasing number of publications in the area illustrates the potential of these species as probes for a variety of diagnostic techniques (fluorescence,[1, 2] ultrasound and photo-acoustic tomography,[3, 4] MRI,[5] PET[6, 7]), and as sensors.[8] Pt(II) and Pd(II) porphyrins, in particular, received great attention due to their oxygen sensing behaviour; thanks to their high phosphorescence quantum yields, long-lived triplet states, large Stokes shifts, and favourable photostability, such species emerged as suitable leads for the development of oxygen probes tailored for a variety of specific applications.[9-12] Optical oxygen sensing relies on the oxygen-dependent decrease of triplet lifetime and phosphorescence intensity, which is caused by the collisional quenching of the phosphor's triplet state. The efficiency of porphyrins as oxygen probes in biological environments is widely documented in the literature. Species such as coproporphyrin and octaethylporphyrin have been successfully employed as stand-alone probes or in conjunction with cell-penetration enhancers to measure intracellular oxygen tension in respiring cells.[13-22] Recently, the association of Pd(II) and Pt(II) porphyrins and benzoporphyrins with dendrimeric structures was reported as a strategy to obtain probes that remain confined to the extracellular compartment, and their efficiency for the measurement of oxygen tension in the intercellular space has been demonstrated.[23-28] The ligation of oxygen-sensing porphyrins with nanoparticles[29-35] and polymers[36-49] has also been explored, as an efficient way to circumvent their low water solubility, and to prevent any undesired interaction of the dye with subcellular structures.

The pivotal importance of measuring oxygen levels and detecting hypoxia gradients has long been recognised in the medical field,[50] but the recent advances in regenerative medicine sparked a renewed interest in the pursuit of innovative strategies for oxygen detection. The need to circumvent some intrinsic disadvantages of electrode-based oxygen sensing methods, which proved detrimental especially for tissue engineering applications, has led to an intense research activity in the field of optical oxygen sensing. Unlike electrode-based methods, optical oxygen sensors cause very limited oxygen depletion in the sample, are minimally invasive and less affected by environmental/experimental conditions,[11, 51] and are amenable to conventional imaging techniques and incorporation into miniaturised devices,[2] and allow simultaneous analysis of multiple samples: thanks to these evidences, the popularity of optical oxygen sensing increased, and progressively more studies featuring optical oxygen sensing for intra- and extracellular oxygen measurements, both in 2D[52-54] and 3D[55-58] cell cultures, appear in the literature.

The regeneration of functional tissue from cell-seeded supports depends on the supply of oxygen and nutrients: an inadequate supply of oxygen to the core cells of an engineered 3D tissue construct leads to the formation of oxygen gradients and hypoxic zones, which can cause the construct to fail. The onset of oxygen gradients in pre-vascularised engineered tissues is governed by the depth of the cell core (gradient length) and the cell density/metabolic activity of cells along that path.[59, 60] The complexity of predicting these factors together with the lack of straightforward methods to measure oxygen gradients,

encouraged the general assumption that all cells sitting deeper than 0.5 mm from the surface will be compromised.[60] Studies conducted in connective tissue, however, indicated that this assumption might be over-pessimistic,[61, 62] and as such, negatively bias or discourage the assessment of the suitability of new materials to sustain cell growth. Straightforward approaches to monitor oxygen gradients are therefore highly desirable to support the design and development of improved materials for 3D engineered tissue constructs.[63]

Unlike amperometric measurements, which probe oxygen tension in the immediate vicinity of the electrode tip, optical oxygen sensing proved able to resolve oxygen gradients in a cell-seeded construct *in situ* and in a non-invasive fashion.[52, 58, 64, 65] Harrington *et al.* showed how an optical probe uniformly distributed in a 3D cell-seeded construct can provide real-time information on the global behaviour of the device during cell growth and migration, using standard luminescence detections and imaging techniques.[57] Following our interest in the sensing applications of porphyrins,[66, 67] we undertook a project aimed at the development of porphyrin-based oxygen nanosensors for incorporation in compressed collagen matrices designed for tissue engineering applications.[60] The use of nanoparticle-supported probes embedded in the matrix prevents the diffusion of the probe molecules, which could lead to cell toxicity. In order to allow the biocompatible ligation of the oxygen sensor to the support of interest (*e.g.*: collagen fibres, polymers, etc.) the desired sensors would need to be: (1) water-soluble and (2) provided with a functional group to allow covalent conjugation to the desired support. Unfortunately, most known oxygen-sensing porphyrins are hydrophobic, and unless suitably derivatised, they can only be dissolved in organic solvents often incompatible with the integrity/functionality of the support (especially biomolecules). Furthermore, the few oxygen-sensing porphyrins which lend themselves to bioconjugation in aqueous media display several copies of the same reactive group, and require further derivatisation to prevent the formation of multiple conjugation products.[68]

In order to circumvent the issues mentioned above, we designed a set of porphyrins bearing (1) charged groups, either positive or negative, to promote water solubility to allow for conjugation in aqueous environment, and (2) a single carboxylic group for selective conjugation in mild, biocompatible conditions (Figure 1). The availability of both positively and negatively charged species allows the choice of the most appropriate sensor for the nature of the matrix in use, to ensure that covalent ligation occurs and avoid the formation of ion pairs with the support (*e.g.*: a negatively charged probe and substrates bearing an overall positive charge).

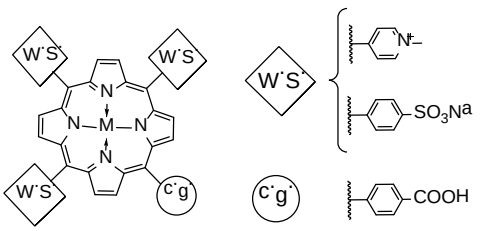

Figure 1: General formula of the water-soluble (W.S.), conjugatable (c.g.) oxygen-sensing porphyrins.

This article describes the synthesis of the new water-soluble mono-functionalised Pt(II) and Pd(II) porphyrin complexes, their conjugation to polyacrylamide nanoparticles, and the assessment of the responsiveness of the species obtained to varying oxygen concentration over a biologically relevant range. We also report the preliminary evidences of the potential of these species as oxygen probes in biomimetic matrices, as shown by the results of oxygen tension measurements performed with nanoconjugates embedded in compressed collagen gels.

Results and discussion

Synthesis

The synthesis of the cationic derivatives **3** and **4** started from the methyl ester of tris-pyridyl-carboxyphenyl porphyrin **1**. (Scheme 1).[69] Metal insertion in meso-pyridyl porphyrins is hampered by the tendency of the pyridyl nitrogens to act as ligands for the metal ion in the macrocycle, leading to the formation of stable tridimensional polymeric complexes.[70-73] Following an approach we previously adopted,[66] we overcame this problem by converting **1** into the corresponding cationic species **2** by treatment with iodomethane in NMP[74] Treatment of **2** with $PdCl_2$ in methanol afforded the desired derivative in good yields. The platinum complexes was prepared following the procedure described by Pasternack *et al.*,[75] which involves refluxing an aqueous solution of the cationic porphyrin in the presence of the labile cationic complex $[Pt(DMSO)_2(H_2O)_2]^{2+}$, prepared in situ by ligand exchange from $Pt(PhCN)_2Cl_2$ upon treatment with DMSO and $AgNO_3$: this method afforded the desired species in 84% yield. Both **3** and **4** were converted into the corresponding free acid by saponification with lithium hydroxide in water.

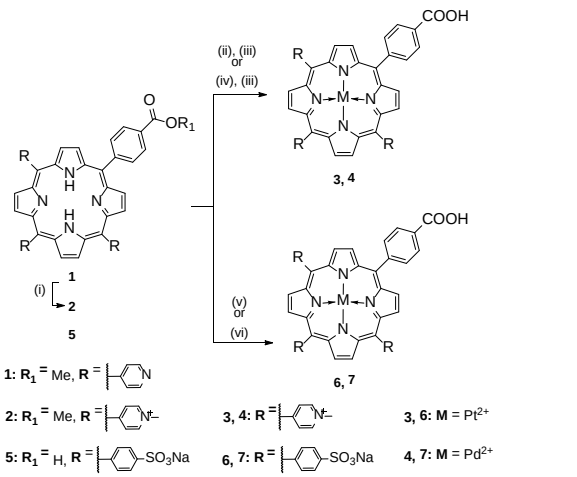

(i) MeI, NMP, 40 °C; (ii): $Pt(DMSO)_2(H_2O)_2$, water, Δ; (iii) LiOH, water; (iv) $PdCl_2$, MeOH, r.t.; (v) $Pt(DMSO)_2(H_2O)_2$, water, μW, 20'; (vi): $Pd(AcO)_2$, water, μW, 5'

Scheme 1

All attempts to generate the platinum and palladium complexes of sulfonated porphyrin **5** under the conditions described above failed; the use of the classic conditions for platinum insertion into porphyrin macrocycles, involving treatment with $Pt(PhCN)_2Cl_2$ in refluxing benzonitrile in an inert atmosphere,[38, 76, 77] was ruled out by the poor solubility of **5** in non-polar solvents. Similarly, palladium insertion by treatment with $PdCl_2$ in refluxing DMF[78] was ineffective because of the lack of solubility of the starting material. Attempts to carry out sulfonation on the platinum or the palladium complexes of 5-(4-carboxyphenyl)-10,15,20-*tris*-phenyporphyrin (*e.g.*: conc. H_2SO_4, 70 °C,[79] or $ClSO_3H$, 40 °C[80]) led to metal loss and/or

degradation of the starting material. Effective conditions to promote metallation of our porphyrins were met when we turned our attention to microwave irradiation (MWI). The use of MWI in organic synthesis has increased considerably over the last decades because it has proved to be a general tool to shorten reaction times and significantly enhance yields and regioselectivity of a wide variety of transformations.[81] Microwave-promoted insertion of group 10 metals in *meso*-tetraarylporphyrins and *meso*-tetraaryl-2,3-dihydroxyporphyrins has been reported previously,[82] but, to the best of our knowledge, it has never been applied to the synthesis of water-soluble derivatives. The water-soluble $Pt(DMSO)_2(H_2O)_2$, prepared following Pasternak's procedure, was transferred in a microwave reactor and irradiated in the presence of **5** at 200 °C over 20 minutes, to yield complex **6**. In similar conditions, MWI of **5** in the presence of water-soluble $PdCl_2$ let to the conversion to **7** within 5 minutes (Scheme 1).

The striking efficiency of this approach compelled us to revisit the synthesis of complex **3**, which was obtained from **2** in 10 minutes and in 90% yield under MWI (*vs.* overnight reflux in conventional heating conditions). The insertion of Pd(II) and Pt(II) in water-soluble porphyrins is sparingly reported in the literature, and the few procedures described are lengthy and low yielding. Furthermore, it is worthy to point out that none of the procedures reported to date was ever adopted for the preparation of conjugatable derivatives. To the best of our knowledge, the MWI-assisted strategy developed in our lab represent the first expeditious and high yielding approach for the synthesis of water-soluble mono-functionalised Pt(II) and Pd(II) porphyrins: the general applicability of this method to otherwise sluggish metal insertion reactions holds the potential to pave the way to novel biomedical applications of porphyrins complexes.

Conjugation of porphyrins **3**, **4**, **6**, and **7** to amino-functionalised polyacrylamide nanoparticles was carried out in water by carbodiimide-mediated coupling in the presence of N-hydroxysuccinimide (Scheme 2).[66, 83] The porphyrin-coated nanospecies **8-11** were obtained in good yields and the dye loading was evaluated spectrophotometrically, on the basis of the molar absorption coefficient of the porphyrins at their absorption maxima. (Table 1). The ligation conditions were optimised using poly(L-lysine) and amino-dextran as models for macromolecular supports (see Supporting Information).

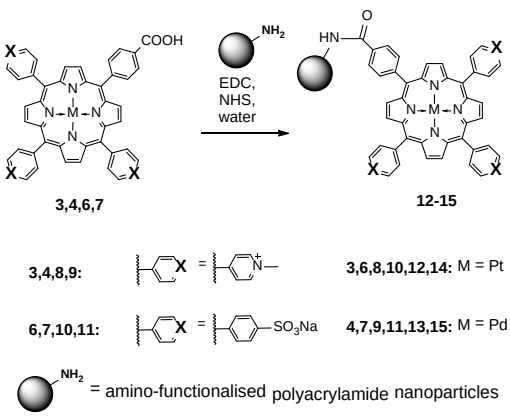

Scheme 2

Table 1: Nanoconjugates recovery yields and loading.

No.	compound	M	yield (%)	loading (nmol/mg)
8	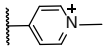	Pt	84	13
9	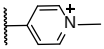	Pd	70	12
10	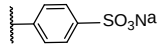	Pt	63	16
11	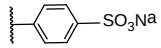	Pd	86	11

Photophysical Characterisation

All the species synthesised are fully water-soluble; their absorption spectra in water show an intense Soret band in the 395–405 nm spectral window, and Q-bands in the 525–545 nm region. The average half-width of the Soret band (>30 nm) for the non-conjugated porphyrins suggests the occurrence of extensive aggregation, a frequently reported behaviour of meso alkylpyridiniumyl and sulfonatophenyl porphyrins in water.[84] Porphyrins **3** and **6** and the corresponding nanoconjugates display the typical blue-shifted Soret bands of Pt porphyrins (Figure 2).[77] As expected, the conjugation to nanoparticles affects the absorptive and emissive behaviour of the chromophores: examples of the absorption and emission spectra are shown in Figure 2 (the complete series of spectra is reported in the Supporting Information). As a general trend, the association to the polyacrylamide support causes a red-shift in the λ_{max} and a broadening of the Soret band, behaviour that can be attributed to dye-support interaction or to self-aggregation of the dye within the polymer.[12, 85]

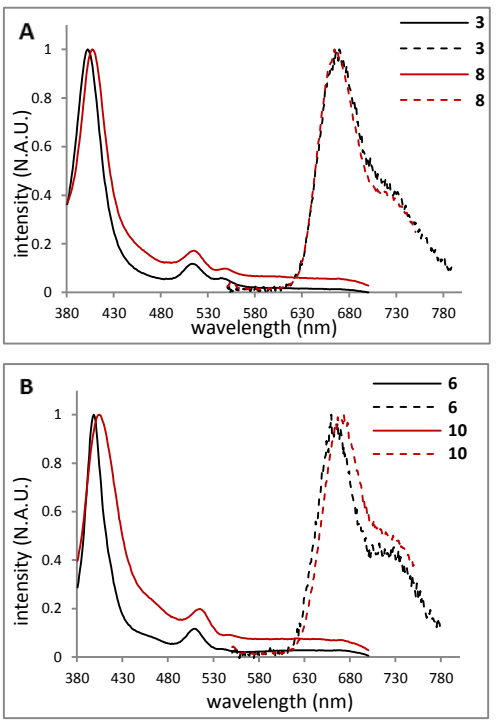

Figure 2: (A): Absorption (solid line) and emission (dashed line) spectra of porphyrin **3** and nanoconjugates **8**; (B): absorption (solid line) and emission (dashed line) spectra of porphyrin **6** and nanoconjugates **10**. Spectra were recorded in deionised water.

Conjugation of the porphyrins to nanoparticles also causes a marked decrease in the triplet state yields, as reflected by the decrease in the singlet oxygen quantum yield, (Table 2), which can be ascribed to enhanced non-radiative decay of the excited states of polymer-supported porphyrins due to dye-matrix interactions. Measurement of triplet lifetime in de-oxygenated aqueous solution shows that the presence of the polyacrylamide matrix does not affect the lifetime of the phosphors, suggesting that triplet decay in the absence of oxygen is not enhanced by the interaction of the porphyrin with the matrix. Longer triplet lifetimes are consistently observed throughout the series for the palladium-containing species **4**, **7** and **9**, **11**.

Prolonged irradiation with continuous red light (645 nm, band width *ca.* 17 nm, > 20 min.) caused a limited reduction of the intensity of the Soret band, both for the porphyrins and the nanoconjugates: (Table 2) this marginal photobleaching is unlikely to hamper the oxygen-sensing performance of these species, as the measurements are normally carried out by exciting the phosphors with significantly lower light doses compared to those used in the present experiments.[86]

Table 2: Photophysical properties of porphyrins and conjugates.

species	λ_{max} (nm)[a]	$\log\varepsilon_{\lambda max}$ (±σ)[a]	λ_{em} (nm)[b]	stability (±σ)[c]	lifetime[d] (μs)	Φ_Δ (±σ)[e]
3	402	5.01 (±0.01)	667	84.5 (± 2.1)	10.0 (± 0.2)	0.72 (±0.07)
4	415	4.97 (±0.01)	700	94.7 (± 1.9)	120.0 (± 3.0)	0.75 (±0.07)
6	398	5.18 (±0.02)	663	94.4 (± 0.9)	30.0 (± 0.1)	0.74 (±0.07)
7	410	5.30 (±0.01)	700	89.7 (± 2.3)	294.0 (± 4.0)	0.76 (±0.07)
8	407	-	664	93.6 (± 0.7)	13.0 (± 0.1)	0.30 (±0.03)
9	410	-	700	94.9 (± 0.4)	95.0 (± 2.0)	0.36 (±0.03)
10	403	-	673	96.8 (± 1.2)	29.0 (± 0.1)	0.32 (±0.03)
11	415	-	700	85.9 (± 1.2)	260.0 (± 4.0)	0.35 (±0.03)

[a]: Soret band, measured in deionised water (±0.1 nm); [b]: (±0.2 nm), $\lambda_{exc.} = \lambda_{max.}$, measured in deionised water; [c]: residual absorbance (%) following 20 min irradiation of an aqueous solution showing an $A(\lambda_{max}) = 1.0$; [d]: $\lambda_{exc.} = 351$ nm, measured in deoxygenated aqueous solutions showing an $A_{351} = 0.1$; [e]: singlet oxygen quantum yield measured in D_2O.

Oxygen sensing: Time-Resolved Domain

The oxygen-induced collisional quenching of phosphorescence is a dynamic process described by the Stern-Volmer relationship (1), stating that the ratio be-tween the triplet lifetime in the absence and the presence of the quencher is linear to the concentration of the quencher.[87]

$$\tau_0/\tau = K_{sv}[O_2] + 1 \quad (1)$$

where τ and τ0 are the triplet lifetime of the chromophore in the presence and in the absence of the quencher, respectively, $[O_2]$ is the molar concentration of oxygen, and K_{sv} is the Stern-Volmer constant, defined as the product of the triplet lifetime in the absence of the quencher and the bimolecular quenching rate constant (i.e.: $K_{SV} = \tau_0 k_q$).

The phosphorescence lifetimes of porphyrins **3**, **4**, **6**, and **7**, and of the porphyrin-decorated nanoparticles **8-11** were determined in aqueous solution at oxygen concentrations ranging from 7.0 x 10^{-4} to 2.7 x 10^{-1} mM (see Supporting Information for experimental details), and the data were processed using a Stern-Volmer type analysis ($1/\tau = k_q[O_2] + 1/\tau_0$) to obtain the bimolecular quenching rate constants, k_q (Table 3). All the species display oxygen-dependent phosphorescence and a good linearity of 1/τ over a biologically relevant oxygen concentration range. The 1/τ vs. O_2 plot for porphyrin **3** is shown in Figure 3 (remaining plots are shown in the Supporting Information). The four porphyrins displayed comparable values of k_q (≈10^9 $M^{-1}s^{-1}$), indicating that for these particular probes, neither the nature of the inner metal nor the charges associated to the macrocycle seem to have a major impact on the efficiency of the collisional quenching of phosphorescence by oxygen. The k_q of the nanoconjugates are one order of magnitude smaller than the ones observed for the corresponding porphyrins (i.e.: ≈10^8 $M^{-1}s^{-1}$), suggesting that the conjugation to polyacrylamide nanoparticles causes a reduction in the oxygen sensitivity of the porphyrin probes: it can be hypothesized that the association with a polymeric support partially shields the phosphor from colliding with molecular oxygen, thereby reducing the efficiency of the quenching.[88, 89]

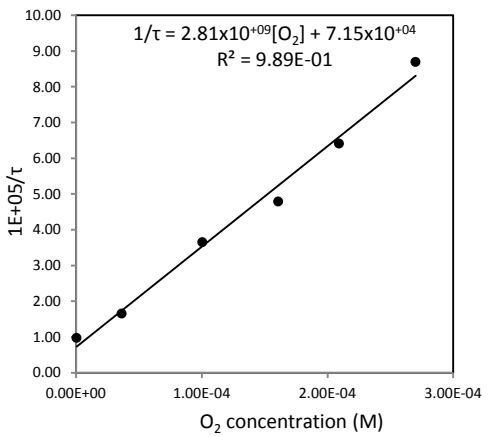

Figure 3: 1/τ vs. O_2 concentration (mM) scatter plot and regression line for porphyrin **3**.

Table 3

species	time resolved			steady state	
	k_q (±σ) (M^{-1} s^{-1})	R^2	k_q (±σ) ($mmHg^{-1}$ s^{-1})	k_q (±σ) (M^{-1} s^{-1})	R^2
porphyrins					
3	2.81×10^9 ($\pm 0.15 \times 10^9$)	0.989	4.76×10^3 ($\pm 0.25 \times 10^3$)	3.06×10^9 ($\pm 0.18 \times 10^4$)	0.986
4	2.46×10^9 ($\pm 0.06 \times 10^9$)	0.997	4.16×10^3 ($\pm 0.11 \times 10^3$)	2.31×10^9 ($\pm 0.07 \times 10^9$)	0.987
6	3.12×10^9 ($\pm 0.07 \times 10^9$)	0.998	5.28×10^3 ($\pm 0.11 \times 10^3$)	2.66×10^9 ($\pm 0.34 \times 10^9$)	0.935
7	2.74×10^9 ($\pm 0.10 \times 10^9$)	0.995	4.64×10^3 ($\pm 0.17 \times 10^3$)	1.79×10^9 ($\pm 0.08 \times 10^9$)	0.992
nanoconjugates					
8	6.27×10^8 ($\pm 0.29 \times 10^8$)	0.985	1.06×10^3 ($\pm 0.05 \times 10^3$)	6.39×10^8 ($\pm 0.25 \times 10^8$)	0.991
9	4.46×10^8 ($\pm 0.11 \times 10^8$)	0.996	7.54×10^2 ($\pm 0.19 \times 10^2$)	5.52×10^8 ($\pm 0.22 \times 10^8$)	0.989
10	1.95×10^8 ($\pm 0.01 \times 10^8$)	0.985	3.29×10^2 ($\pm 0.15 \times 10^2$)	2.64×10^8 ($\pm 0.27 \times 10^8$)	0.995
11	1.85×10^8 ($\pm 0.05 \times 10^8$)	0.994	3.14×10^2 ($\pm 0.09 \times 10^2$)	2.05×10^8 ($\pm 0.05 \times 10^8$)	0.995

Bimolecular quenching constants and correlation coefficients for porphyrins **3**, **4**, **6**, and **7**, and nanoconjugates **8-11** over the oxygen concentration range 7×10^{-4} to 2.7×10^{-1} mM. ([a]: value extrapolated from the calibration line)

Oxygen sensing: steady state measurements

According to the Stern-Volmer equation, in the presence of purely dynamic quenching:

$$I_0/I = \tau_0/\tau = K_{sv}[O_2] + 1 \quad (\text{where: } K_{SV} = \tau_0 k_q) \qquad (2)$$

where I_0/I is the ratio of the phosphorescence intensity in the absence (I_0) and in the presence (I) of the quencher. According to Eq. 2, calibration of the sensor and oxygen tension measurements can be based on the quenching of the phosphorescence emission rather than the triplet lifetime. Although steady-state measurements of quencher concentration are less sensitive and more easily affected by the experimental conditions and by environmental factors (*e.g.*: phosphor concentration, background fluorescence, etc.), whenever applicable, they allow the use of simpler and cheaper instrumentation. Steady-state oxygen measurement have been successfully applied to cultured cells,[12, 34] *in vivo*,[90, 91] and also found applications in microfluidic devices.[92, 93] With the exception of porphyrin **6**, for which the correlation coefficient for the linear regression is lower, all porphyrins and nanoconjugates display linear relationships between I_0/I and oxygen concentration, throughout the range 7.0×10^{-4} - 2.7×10^{-1} mM (Table 3). Figure 3 shows the emission spectra of porphyrin **3** at different concentration of oxygen (A), and the corresponding scatter plot and regression line (B).
Figure 5 shows the intensity and lifetime Stern-Volmer plots for porphyrin **3**, and Table 4 reports the data obtained for all the species (remaining Stern-Volmer plots are provided in the Supporting Information). In most of the cases there is good agreement between the values of the K_{SV} values of the lifetime and intensity plots, indicating that the predominant pathway of triplet deactivation for these species under the experimental conditions de-scribed is due to dynamic quenching by oxygen, and that no static quenching is involved.

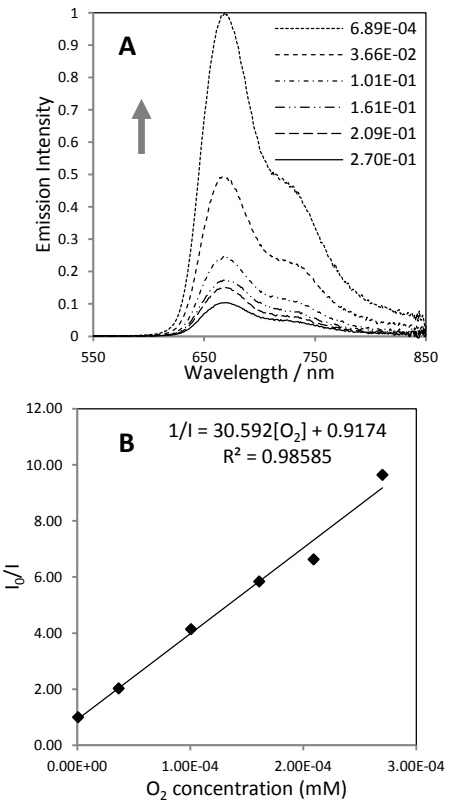

Figure 4: Fluorescence emission profiles (A) and I_0/I Stern-Volmer plot (B) for porphyrin **7** (arrow indicates decreasing O_2 concentration).

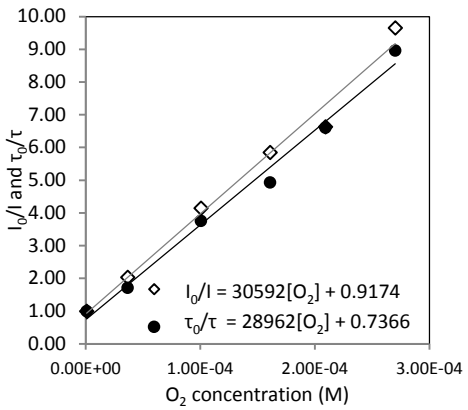

Figure 5: Lifetime (●) and intensity (◇) Stern-Volmer plots for porphyrin **3**.

All probes exhibit a marked enhancement of phosphorescence intensity and triplet lifetime in deoxygenated- compared to air-saturated solutions; the free porphyrins display larger I_0/I and τ_0/τ ratios than the corresponding nanoconjugate, and similarly, the I_0/I and τ_0/τ values observed for Pd(II) complexes are higher than the ones found for the corresponding Pt(II) species, confirming that larger values of τ_0 confer higher oxygen sensitivity on the probes. The linearity of time-resolved and steady-state responses over a biologically relevant oxygen concentration range shows the suitability of these porphyrin-based probes for oxygen measurements in the biomedical field.

Table 4

species	time resolved			steady state		
	K_{SV} (±σ)	R^2	τ_0/τ_{min}	K_{SV} (±σ)	R^2	I_0/I_{min}
porphyrins						
3	3.06×10^4 ($\pm 0.18 \times 10^4$)	0.989	8.96	2.90×10^4 ($\pm 0.18 \times 10^4$)	0.986	9.65
4	2.95×10^5 ($\pm 0.08 \times 10^5$)	0.997	82.2	2.78×10^5 ($\pm 0.08 \times 10^5$)	0.987	72.73
6	9.33×10^4 ($\pm 0.19 \times 10^4$)	0.998	25.8	8.15×10^4 ($\pm 1.07 \times 10^4$)	0.935	23.18
7	8.07×10^5 ($\pm 0.29 \times 10^5$)	0.995	213.04	5.26×10^5 ($\pm 0.24 \times 10^5$)	0.992	140.87
nanoconjugates						
8	8.28×10^3 ($\pm 0.39 \times 10^3$)	0.985	3.30	7.89×10^3 ($\pm 0.33 \times 10^3$)	0.991	3.17
9	6.06×10^4 ($\pm 0.15 \times 10^4$)	0.996	17.74	5.54×10^4 ($\pm 0.21 \times 10^4$)	0.989	14.90
10	5.60×10^3 ($\pm 0.26 \times 10^3$)	0.985	2.46	7.66×10^3 ($\pm 0.77 \times 10^3$)	0.995	2.99
11	4.82×10^4 ($\pm 0.38 \times 10^4$)	0.994	13.68	5.43×10^4 ($\pm 0.14 \times 10^4$)	0.995	15.87

Data for the lifetime and intensity Stern-Volmer plots for the oxygen-sensing porphyrins and nanoconjugates.

Oxygen sensing in compressed collagen scaffolds

The promising oxygen-sensing behaviour shown by the sensors encouraged us to undertake a study to investigate the possibility of employing the nanoconjugates to monitor oxygen diffusivity in 3D collagen matrices. To this aim, we embedded nanoconjugate **9** in compressed rat tail Type I collagen matrices. The compressed collagen matrix has a much lower water content and therefore higher collagen density than uncompressed collagen hydrogel. The collagen density of *ca.* 11% w/w is comparable with that found in tissues, which makes these compressed gels excellent biomimetic matrices. The compressed matrices were shaped into rods and suspended in 0.01 M PBS solution in a sealed quartz cuvette, and the oxygen concentration in the medium was varied by streaming nitrogen through the solution.[1, 94] A calibrated fibre-optic oxygen sensing probe was placed halfway along the length of the rod's longitudinal axis, with the purpose of verifying the equilibration of oxygen levels during nitrogen degassing and to provide a comparison measurement. Time-resolved phosphorescence signals from the embedded nanosensors were detected using a fibre-optic probe placed adjacent to the surface of the collagen matrix (Figure 6 and Supporting Information).

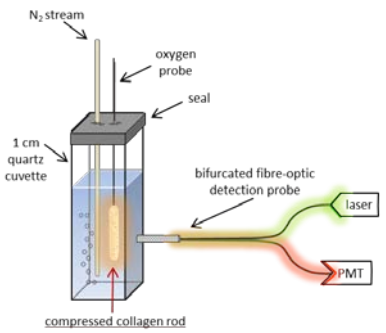

Figure 6: Experimental setting for oxygen sensing in com-pressed collagen rods.

Figure 7 shows the phosphorescence decay of the nanoconjugate in the compressed collagen gel (A) and the linear Stern-Volmer plot of lifetime decay (B) at different levels of oxygen, illustrating the efficiency of this nanoconjugate for oxygen sensing in a biomimetic collagen matrix and its potential for applications in 3D constructs. The lower value of K_{SV} observed in the collagen matrix (see Figure 7, A and B) is ascribable to two main factors, namely (1) the faster oxygen diffusion in solution compared to the collagen gel,[62] and (2) the dye-matrix interaction which partially shields the phosphors from interactions with the surrounding environment. The triplet lifetime shows a three-fold increase (τ_0/τ min) from the highest oxygen concentration examined to the deoxygenated sample, providing the

necessary sensitivity over the dynamic range of interest. We also observed that the conjugates were well retained in the collagen matrix and no significant leaching into the PBS solution occurred: no detectable phosphorescence was observed in the PBS solution using the same optical configuration following removal of the collagen sample.

From these data it emerges that nanoconjugate **9** maintain their oxygen responsiveness in a relatively complex and heterogeneous environment such as compressed collagen. These preliminary evidences point out the potential of these species as oxygen concentration reporters in cell-seeded tissue models, where, unlike fibre-optic probes and electrodes, they could provide a real-time 3D map of oxygen distribution throughout the support and assist in evaluating the rate of oxygen diffusion and oxygen consumption by the cells.

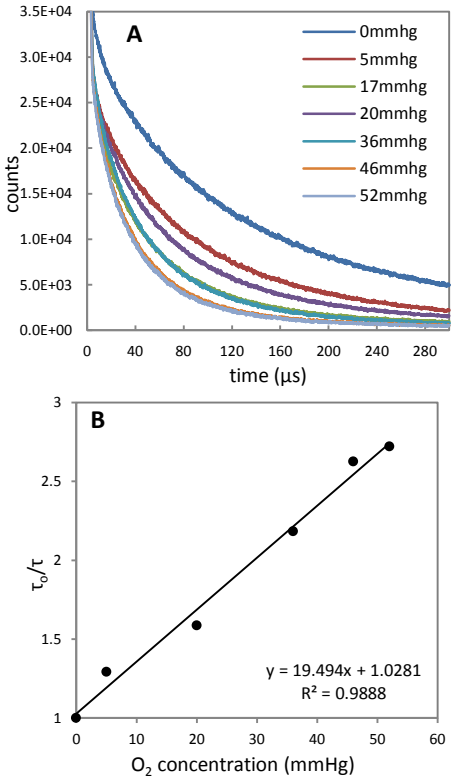

Figure 7: Triplet lifetime decay (A) and corresponding Stern-Volmer plot (B) of nanoconjugate **9** embedded in collagen matrix over the 0-52 mmHg oxygen tension range (corresponding to 0 – 8.84 x 10^{-2} mM). Stern-Volmer constant is K_{SV}=0.0958 $mmHg^{-1}$ (19.494 mM^{-1}) and the bimolecular quenching rate constant is k_q=355 $mmHg^{-1}s^{-1}$ (R^2=0.9955).

Conclusions

Novel water-soluble oxygen-sensing phosphors based on Pt(II) and Pd(II) complexes of porphyrins were synthesised. The molecules were designed to bear charged moieties and a single carboxylic group to ensure water solubility and to prevent the formation of cross-linked conjugates, respectively, making these species extremely versatile towards ligation with amino-functionalised substrates of different chemical nature; in particular, the ligation of the probes to bio-macromolecules is feasible owing to the possibility of performing the conjugation in aqueous solutions and in mild conditions. To achieve the metal insertion of Pt(II) and Pd(II) in the free water-soluble macrocycles, we developed a microwave-assisted method that rapidly affords the desired species in high yields. Ligation to amino-functionalised polyacrylamide nanoparticles gave nanoconjugates with loading ratios varying between 11 and 13 nmol/mg. All species display oxygen-dependent phosphorescence in time-resolved domain and steady state, with triplet lifetimes and emission intensities varying linearly with the oxygen concentration, over a physiologically relevant range. Importantly, we showed that the nanoprobes can be easily incorporated and retained in a compressed collagen gel, where their oxygen-sensing behaviour is maintained. These data encourage the use of the sensors as investigative tools to monitor the oxygen flow in matrices for tissue regeneration construct. The incorporation of the oxygen sensing porphyrins within ratiometric and/or dual nanosensors (*e.g.*: oxygen and pH sensors), and the covalent ligation of the molecular probes to the scaffold matrix are currently under investigation in our laboratories.

Experimental Section

General Remarks: ^{1}H and ^{13}C NMR spectra were recorded on JEOL Eclipse 400 and JEOL Lambda 400 spectrometers (operating at 400 MHz for 1H and 100 MHz for ^{13}C). $CDCl_3$, DMSO-d_6, and MeOH-d_3 were used as solvents. Chemical shifts (δ) are reported in parts per million (ppm), referenced to either $CHCl_3$ (^{1}H, 7.26 ppm; ^{13}C, 77.16 ppm) or DMSO (^{1}H, 2.50 ppm; ^{13}C, 39.52 ppm) or MeOH (^{1}H, 3.31 ppm; ^{13}C, 49.00 ppm). Coupling constants (J) are recorded in Hz and significant multiplicities described by singlet (s), doublet (d), triplet (t), quadruplet (q), broad (br), multiplet (m), or doublet of doublets (dd). A Malvern Photon Correlation Spectrometer equipped with a 70 mW blue laser operating at 470 nm at an angle of 90° was used for the PCS measurements. The measurements were performed at room temperature, at a concentration of 5 mg/mL of nanospecies in 7 mM aqueous NaCl, unless otherwise stated, and the solutions were filtered through a 0.22 µm filter (Millex GP) previous to the measurements. ESI mass spectra were performed on a Thermofisher LTQ orbitrap XL (EPSRC Mass Spectrometry Service, Swansea), or on a Varian 500-MS ion trap spectrometer, equipped with a Varian Prostar 212LC binary gradient pumping system and a Varian ProStar 410 autosampler. A standard Varian ESI source was used operating in +ve ion mode. Data was acquired and processed using Varian Workstation software. MALDI mass spectra were performed on a Bruker Reflex IV MALDI-TOF, operated in reflectron mode and monitoring positive ions. Data was acquired and processed using Bruker Compass software. 1,8-Dihydroxy-9,10-dihydroanthracen-9-one (dithranol) was used as the matrix. UV−visible spectra were recorded on a Varian Cary 50 UV/vis spectrophotometer (wavelength accuracy: ± 0.24 nm). Fluorescence spectra (uncorrected) were recorded on a Cary Eclipse Fluorimeter. The singlet $^{\Delta}$oxygen quantum yield, Φ_{Δ}, was determined using by time-resolved phosphorescence measurements.[95, 96] Samples dissolved in D2O and allowed to equilibrate with air and were excited using the third harmonic of a Q-switched Nd:YAG laser (355 nm). A CuSO4 filter was used upstream of the solution to remove residual 1064 nm radiation in the pump beam. Typical pulse energies used were in the range 0.1–1 mJ per pulse. A North Coast E0-817P Ge photodiode/amplifier combination detected the singlet oxygen phosphorescence at right angles to the incident laser beam. The sample was placed in a fluorescence cuvette with a 10 mm path length close to the detector. The singlet oxygen luminescence was selected with a 1270 nm silicon interference filter (bandpass, 30 nm) placed close to the detector. Singlet oxygen

quantum yields were determined relative to rose Bengal (Φ_Δ = 0.76). Photostability experiments were carried out with a LED source, with 126 diodes arranged equally in a panel of 10 X 16 cm. The power is 50W/m^2 at the working distance, and the peak maximum is 642 nm (spectrum reported in the Supplementary Information). Flash chromatography was carried out on silica gel 60 (MP Biomedicals, 32−63 μm). Analytical TLC was carried out on aluminium sheets pre-coated with silica gel 60 (Fluka, 0.2 mm thick). Reactions under microwave irradiation were performed in a CEM Discovery SP-D at a power of 100 W. Chemical reagents were purchased from Sigma-Aldrich, Fluka, Acros, Lancaster, and Alfa Aesar at the highest grade of purity available, and were used as received unless otherwise stated. Dichloromethane and THF were dried by filtration through alumina and stored over activated molecular sieves.[97] All other solvents were purchased from Fisher Scientific and used as received. Argon and oxygen gas gases were purchased from BOC Gases (Manchester, United Kingdom). Deionized water (18.2 MΩ) was generated by Elga Purelab Ultra (ULXXXGEM2) or from a Millipore Milli-Q system. Gel filtrations were performed on Sephadex® G-25 medium, using pre-packed PD-10 columns (GE Healthcare, UK), using deionised water as the eluent. Filtrations through membranes were performed on Sartolon® polyamide filters, 25 mm, 0.20 μm pores. Solid phase extractions were performed on Supelco Discovery DSC-18 cartridges (1 g). RP-HPLC analyses were performed on a system consisting of a Perkin Elmer series 200 LC pump, and a Perkin Elmer 785A UV/vis detector. The separations were performed on a Gemini C18, 5 μ, 150 x 4.6 mm, 110 Å (Phenomenex, UK), equipped with a SecurityGuard C18 (ODS) 4 x 3.0 mm ID guard column (Phenomenex, UK) at a flow rate of 1 mL/min. Method A: the mobile phase consisted of 0.1% TFA in water (solvent A) and 0.1% TFA in acetonitrile (solvent B). Gradient: 0.0–10.0 min, 0-95% B; 10.0–15.0 min, 95% B; 15.0–15.1 min, 95-5% B; 15.1–18.0 min, 5% B. Method B: the mobile phase consisted of 0.1 M NH4AcO in water (solvent A) and 0.1 M NH_4AcO in 50% aqueous AcCN (solvent B). Gradient: 0–15.0 min, 2-100%, B; 15.0–18.0 min 100%, B; 18.0–18.1 min, 100-2% B; 18.1–20.0, min 2% B. Amino-functionalised polyacrylamide nanoparticles were obtained according to methods reported in the literature.[67, 98] 5-(4-carboxymethylphenyl)-10,15,20-tris(4-methylpyridinium)porphyrin trichloride,71 and 5-(4-carboxymethylphenyl)-10,15,20-tris(4-sulfonatophenyl)porphyrin trisodium[99] were synthesised according to methods reported in the literature.

Oxygen concentration measurements in time-resolved domain. Phosphorescence lifetimes were recorded using a time-correlated photon counting spectrometer. The samples were held in a four-sided quartz cuvette equipped with a degassing bulb. The samples were excited using the output of a pulsed nitrogen laser (VSL-337i OEM), which provided a 10Hz pulse train of pulse duration < 5 ns at 337 nm, with a pulse energy of ca. 5 μJ. Emission was collected at 90° to the excitation source and the emission wavelength was selected using a monochromator (Bentham TM300) and the selected light detected using a red-sensitive photon counting photomultiplier module (Hamamatsu H10682-1). The arrival times of multiple photons were recorded from each laser shot using a multi-channel scaler, and the data from a minimum of 10,000 laser shots was acquired to furnish the emission decay. Prior to measurements the sample was completely degassed by a series of freeze-pump-thaw cycles. Once degassed the concentration of oxygen in the sample cell was adjusted by back-filling the cell with a known pressure of air and according to Henry's Law, $[O_2] \propto$ pair. In this way the concentration of oxygen could be varied from 0 – 0.27 M.

Oxygen concentration measurements under steady-state conditions. Dissolved oxygen concentrations were measured using an OceanOptics NeoFox (NFB0181) fluorescence-based optical sensor probe which was immersed in solutions of oxygen-sensitive fluorophores (0.01 mg/mL, 10 mL) and suspensions of oxygen-sensitive nanoparticles (0.50 mg/mL, 10 mL) in deionised water. The dissolved oxygen concentration of these solutions/suspensions was varied by bubbling in argon and oxygen gas, representing 0% and 100% oxygen concentration, respectively. Oxygen-dependent fluorescence intensities of samples were recorded using a Varian Cary Eclipse fluorescence spectrophotometer. Table 5 shows excitation and emission wavelengths used to determine oxygen-dependent fluorescence response. For dissolved oxygen concentrations below atmospheric oxygen concentrations stirring samples were deoxygenated by bubbling in argon gas. Once the samples were deoxygenated the argon source was removed and the samples were allowed to re- equilibrate to atmospheric oxygen concentrations. For oxygen concentration above atmospheric oxygen concentrations, stirring samples were oxygenated by bubbling in oxygen gas. Once the samples were fully oxygenated the oxygen source was removed and the samples were allowed to equilibrate to atmospheric oxygen concentrations. Fluorescence spectra of re-equilibrating samples were taken at regular intervals, from which an oxygen-dependent fluorescence response was determined.

Table 5

species	λ_{exc} (nm)	λ_{em} (nm)	λmax_{em}-λmax_{exc} (nm)
3	400	670	270
4	415	700	285
6	400	665	265
7	410	700	290
8	405	665	260
9	410	715	305
10	405	670	265
11	415	705	290

Oxygen concentration measurements in collagen sheets. Compressed collagen matrix construction: The gels were prepared with 80% (by volume) of rat tail collagen type I (First Link Ltd, UK) with a protein concentration of 2.05 mg/ml in 0.6% acetic acid, 10% 10x Eagles MEM solution (Gibco Chemicals, UK) and 10% 20 μM of nanoparticle sample 9 in 0.01M Dulbecco's Phosphate Buffered Saline (PBS). Gels without nanoparticles were also prepared as controls with 80% rat tail collagen, 10% 10x MEM and 10% PBS. The mixture was neutralised with 5 M NaOH based on the indicator colour changes and placed in an aluminium mould of 2.2x3.3x1 cm dimensions. The mixture was then incubated for 30 minutes to allow the gel to set. The collagen gel was then compressed between two nylon meshes to reduce the water content for 5 minutes giving a flattened sheet approximately 50 μm thick. The sheet was rolled tightly to produce a cylindrically shaped rod of approximately 2 mm diameter and 20 mm length.[60]

Setup for oxygen and luminescence measurements.[60] A thin fibre-optic oxygen sensing probe (Oxylab pO_2 E Series sensor, Oxford Optronix Ltd.) was inserted halfway along the longitudinal axis of the folded collagen gel. The gel containing the probe was transferred into a PBS solution within a 1 cm square quartz cuvette with the collagen surface placed adjacent to one of the cuvette walls. The cuvette was sealed with a plastic film to prevent re-oxygenation of the sample during the deoxygenation procedure. During the measurements a magnetic stirrer was used to keep the oxygen concentration homogenous in the solution. The removal of oxygen was performed by bubbling the solution with oxygen-free nitrogen gas (BOC Ltd) introduced via a hypodermic needle inserted through the film sealing the cuvette, placed adjacent to the gel. The oxygen concentration within the gel was then adjusted to the desired partial pressure and allowed to stabilise.

Time Resolved Luminescence Decay Measurements: The phosphorescence decays were measured using time resolved photon counting. The samples were excited using a 532 nm passively Q-switched diode-pumped solid state Nd:YAG laser (Lumanova GmbH, Germany) with the beam focused into a bifurcated fibre-optic coupler with an SMA termination (Avantes BV). The laser was pulsed at a repetition rate of 2.8 kHz and a pulse length of 3 ns, with a mean power of c. 0.5 mW at the fibre probe tip giving a spot size of c. 1 mm diameter on the gel. A fast photodiode (1 ns rise time, PDM-400, Becker-Hickl, Berlin, Germany) was used to synchronise the laser pulse with the photon counting detection system. Excitation light from the laser was delivered through one arm (400 micron core) of the bifurcated fibre-optic bundle.

5-(4-Methoxycarbonylphenyl)-10,15,20-tris(4-methylpyridinium)porphyrinato platinum (II) tri-chloride: The water-soluble $Pt(DMSO)_2(H_2O)_2$ was synthesised according to a modification of the procedure reported by Pasternack et al..[75] A suspension of platinum dibenzonitrile dichloride[100] (524 mg, 1.11 mmol) in DMSO (5 mL) was stirred at room temperature for 3 hours. De-ionised water (10 mL) was added to the solution, and the resulting suspension was treated with 2 (300 mg, 0.37 mmol) and silver nitrate (189 mg, 1.11 mmol). The mixture was protected from light and stirred at room temperature for 3 h. Silver chloride was then removed by filtration through celite, the mixture was transferred to a microwave reaction vessel equipped with a stirring bar, flushed with argon for 10 minutes and exposed to microwave heating (200 °C, 100 mW, 10 min). The reaction mixture was diluted with deionised water and filtered through celite. The filtrate was treated with a 10% aqueous solution of NH_4PF_6, leading to the precipitation of the porphyrin. The precipitate was collected by centrifugation and dissolved in acetone. The resulting solution was treated with 10% TBAC in acetone to induce the precipitation of the title compound, which was collected by centrifugation, washed with acetone, and further purified by crystallisation from methanol/diethyl ether. (Brick red. 340 mg, 90%). M.p.(°C): > 300. HPLC (Method A): t_R: 7.20; ^{1}H NMR: (d_6-DMSO) δ: 9.44-9.41 (6H, *10+15+20-m-Ar*), 8.95 (br, 6H, *β-H*), 8.90-8.81 (m, 8H, *β-H* and *10+15+20-o-Ar*), 8.35 (2H, d, *J* 8.2, *5-o-Ar*), 8.25 (2H, d, *J* 8.2, *5-m-Ar*), 4.64-4.57 (m, 9H, NCH_3), 3.97 (s, 3H, COOCH_3); ^{13}C NMR: (d_6-DMSO) δ: 166.3, 155.5, 144.4, 140.6, 139.3, 139.2, 138.9, 134.0, 131.7, 129.8, 128.1, 123.2, 117.8, 117.5, 52.6, 47.9; MALDI-MS (+ve, dithranol) (m/z): calcd. for $C_{46}H_{36}N_7O_2Pt$: 913.267, found: 913.361 [M- 3Cl]$^+$; UV/vis: (H_2O) λ (%): 404 (100), 513 (11.9), 543 (4.5); log ε_{421}: 5.10

5-(4-Methoxycarbonylphenyl)-10,15,20-tris(4-methylpyridinium)porphyrinato palladium (II) tri-chloride 3: To a solution of **2** (220 mg, 0.27 mmol) in 1-methylpyrrolidin-5-one (10 mL) Pd(II) diacetate (360 mg, 0.53 mmol) was added as a solution in methanol (3 mL). The mixture was purged with Ar for 5 minutes, then it was heated at 50 °C for 1 hour, cooled at room temperature and filtered through celite. Diethyl ether (100 mL) was added to the filtrate and the resulting suspension was filtered through paper. The precipitate was dissolved in water and the resulting solution was treated with 10% aqueous NH_4PF_6. The precipitate was collected by centrifugation and dissolved in acetone. The resulting solution was treated with 10% TBAC in acetone to induce the precipitation of the title compound, which was collected by centrifugation, washed with acetone, and further purified by crystallisation from methanol/diethyl ether. (201 mg, 80%). M.p.(°C): > 300. HPLC: t_R: 7.16; ^{1}H NMR: (d_6-DMSO) δ: 9.55-9.51 (6H, *10+15+20-m-Ar*), 9.10 (br, 4H, *β-H*), 9.02-8.95 (m, 10H, *β-H* and *10+15+20-o-Ar*), 8.38 (2H, d, *J* 7.8, *5-o-Ar*), 8.33 (2H, d, J 7.8, *5-m-Ar*), 4.73-4.71 (m, 9H, NCH_3), 4.05 (s, 3H, COOCH_3); ^{13}C NMR: (d6-DMSO) δ: 166.3, 155.9, 144.7, 144.3, 141.2, 139.9, 139.8, 139.6, 134.2, 132.7, 132.3, 132.1, 131.8, 129.8, 128.0, 122.7, 117.2, 116.8, 52.6, 47.8; MALDI-MS(+ve, dithranol) (m/z): calcd. for $C_{45}H_{34}N_7O_2Pd$: 824.19, found: 824.19 [M- 3Cl]$^+$; UV/vis: (H_2O) λ (%): 419 (100), 529 (10.2), 565 (3.4); log ε_{421}: 5.29

General procedure for the hydrolysis of methyl ester (A). 5-(4-Carboxyphenyl)-10,15,20-tris(4-methylpyridinium)porphyrinato platinum (II) trichloride 3: A solution of porphyrin 5-(4-methoxycarbonylphenyl)-10,15,20-tris(4-methylpyridinium)porphyrinato platinum (II) tri-chloride (100 mg, 0.10 mmol) in deionised water (5 mL) was treated with LiOH (44 mg, 0.98 mmol). The mixture was stirred at room temperature for 30 minutes, and then it was diluted with water (20 mL). The resulting solution was treated with a 10% aqueous solution of NH_4PF_6, leading to the precipitation of the porphyrin. The precipitate was collected by centrifugation and dissolved in acetone. The resulting solution was treated with 10% TBAC in acetone to induce the precipitation of the title compound, which was collected by centrifugation, washed with acetone, and further purified by crystallisation from methanol/diethyl ether. M.p.(°C): > 300. HPLC (Method A): t_R: 6.49 min; ^{1}H NMR: (d_6-DMSO) δ: 9.36-9.33 (6H, m, *10+15+20-m-Ar*), 8.91 (s, 6H, *β-H*), 8.87-8.80 (m, *8H*, *β-H* and *10+15+20-o-Ar*), 8.19 (2H, d, *J* 8.2, *5-o-Ar*), 7.95 (2H, d, *J* 8.2, *5-m-Ar*), 4.61 (s, 9H, NCH_3); ^{13}C NMR: (d_6-DMSO) δ: 180.6, 155.7, 144.4, 141.1, 140.8, 139.6, 139.1, 138.6, 137.5, 133.9, 132.9, 131.8, 131.5, 131.0, 129.4, 126.1, 125.9, 117.6, 117.0, 57.4, 48.0; MALDI-MS(+ve, dithranol) (m/z): calcd. for $C_{45}H_{34}N_7O_2Pt$: 899.24, found: 899.29 [M-3Cl]$^+$; UV/vis: (H_2O) λ (%): 402 (100), 514 (10.0), 543 (4.5); log ε_{402}: 5.01

5-(4-Carboxyphenyl)-10,15,20-tris(4-methylpyridinium)porphyrinato palladium (II) tri-chloride 4: The species was synthesised according to the general procedure A. Scale: 0.10 mmol. Yield: 81%, 80 mg, brick-red solid. M.p.(°C): > 300 . HPLC (Method A): t_R: 6.53 min; 1H NMR: (d_6-DMSO) δ: 6.48-6.47 (6H, m, *10+15+20-m-Ar*), 9.07 (4H, s, *β-H*), 8.97 (10H, s, *β-H* and *10+15+20-o-Ar*), 8.26 (2H, d, *J* 6.9, *5-o-Ar*), 8.03 (2H, d, *J* 6.9, *5-m-Ar*), 4.67 (s, 9H, NCH_3); ^{13}C NMR: (d_6-DMSO) δ: 167.7, 156.1, 144.3, 141.7, 139.9, 139.5, 133.2, 133.0, 132.1, 131.8, 131.5, 127.7, 117.1, 116.3, 47.8; MALDI-MS (+ve, dithranol) (m/z): calcd. for

$C_{46}H_{36}N_7O_2Pt$: 913.267, found: 913.361 [M- 3Cl]$^+$; UV/vis: (H_2O) λ (%): 417 (100), 525 (11.5), 560 (5.1); log ε_{417}: 4.97

5-(4-Carboxyphenyl)-10,15,20-tris(4-sulfonatophenyl)porphyrinato platinum(II) trisodium 6: A suspension of platinum dibenzonitrile dichloride (140 mg, 0.30 mmol) in DMSO (1.2 mL) was stirred at room temperature for 3 hours. Deionised water (10 mL) was added to the solution, and the resulting suspension was treated with silver nitrate (101 mg, 0.60 mmol), protected from light and stirred at room temperature for 3 h. Silver chloride was then removed by filtration through celite, and the mixture was transferred to a microwave reactor equipped with a stirring bar. **5** (160 mg, 0.16 mmol) was added to the solution; the mixture was flushed with argon for 10 minutes and exposed to microwave heating (200 °C, 100 mW, 20 min). Upon cooling, the solution was filtered through celite, and the porphyrin was recovered by filtration following precipitation with acetone. The precipitate was dissolved in a 1 mM aqueous sodium hydroxide, and precipitated with acetone. The solid was taken in water, purified by solid phase extraction, the eluate was evaporated to dryness and the desired compound was crystallised from methanol/diethyl ether. (Brown/red solid, 181 mg, 97%). M.p.(°C): > 300. HPLC (Method B): t_R: 8.98; ^{1}H NMR: (d_6-DMSO) δ: 8.72-8.67 (8 H, m, *β-H*), 8.31 (2H, d, *J* 8.2, *5-o-Ar*), 8.24 (2H, d, *J* 8.2, *5-o-Ar*), 8.08 (6H, d, *J* 8.0, *10+15+20-m-Ar*), 7.98 (6H, d, *J* 8.0, *10+15+20-o-Ar*); ^{13}C NMR: (d_6-DMSO) δ: 170.3, 167.4, 147.9, 144.7, 140.4, 140.1, 140.0, 133.8, 133.1, 131.1, 130.9, 130.7, 128.1, 124.3, 122.2, 122.1, 121.3; ESI-MS (-ve) (m/z): calcd. for $[C_{45}H_{25}N_4O_{11}PtS_3]^{3-}$/3: 363.0120, found: 363.0106 [M- 3Na]$^{3-}$/3; UV/vis: (H_2O) λ (%): 398 (100), 509 (9.5), 541 (1.9); log ε_{398}: 5.18

5-(4-Carboxyphenyl)-10,15,20-tris(4-sulfonatophenyl)porphyrinato palladium(II) trisodium 7: 80 A solution of **5** (200 mg, 0.21 mmol) and palladium dichloride (73 mg, 0.41 mmol) in methanol (10 mL) in a microwave reactor vessel was purged with Ar for 10 minutes and exposed to microwave heating (90 °C, 100 mW, 10 min). Upon cooling, the mixture was filtered through celite and evaporated to dryness. The solid was taken up in 1 mM aqueous NaOH and the porphyrin was precipitated with acetone, and collected by filtration. The solid was taken in water, purified by solid phase extraction, and the eluate was evaporated to dryness. The desired compound was crystallised from methanol/diethyl ether. (Brick red solid, 220 mg, 98%). M.p.(°C): > 300. HPLC (Method B): t_R: 9.09; ^{1}H NMR: (d_6-DMSO) δ: 8.82-8.78 (8 H, m, *β-H*), 8.36 (2H, d, *J* 8.0, *5-o-Ar*), 8.29 (2H, d, *J* 8.0, *5-o-Ar*), 8.14 (6H, d, *J* 8.0, *10+15+20-m-Ar*), 8.04 (6H, d, *J* 8.0, *10+15+20-o-Ar*); ^{13}C NMR: (d_6-DMSO) δ: 167.5, 147.8, 144.9, 140.9, 140.8, 140.4, 134.0, 133.2, 131.4, 131.2, 127.9, 124.3, 121.6, 121.5, 120.8; ESI-MS (-ve) (m/z): calcd. for $[C_{45}H_{25}N_4O_{11}PdS_3]^{3-}$/3: 332.9914, found: 332.9907 [M- 3Na]$^{3-}$/3; UV/vis: (H_2O) λ (%): 411 (100), 521 (9.1), 556 (1.7); log ε_{411}: 5.30

General procedure for the conjugation of amino-reactive porphyrins to amino-functionalised sub-strates: Nanoconjugates 8. A solution of porphyrin **3** (2 mg, 2.0 x 10^{-3} mmol) in deionised water was treated with EDC (2 mg, 1.0 x 10^{-2} mmol) and NHS (2 mg, 1.7 x 10^{-2} mmol) and allowed to stand at room temperature for 30 minutes. The solution was then added to a dispersion of amino-functionalised nanospecies (100 mg) in deionised water (20 mL). The resulting mixture was shielded from light and shaken for 8 hours on a rotating shaker. The desired conjugated species were purified by gel filtration. Ethanol was added to the eluate, and the particles were isolated by filtration through membrane and dried in vacuo (light orange-red solid, 62 mg, 62% recovery). PCS: Z_{ave} (nm) 75.9±5.5; UV/vis: (H_2O) λ (%): 407 (100), 515 (22.9), 541 (16.9)

Nanoconjugates 9. The conjugated nanospecies were obtained following the general procedure, using amino-functionalised nanospecies (100 mg) and porphyrin 4 (3 mg, 3.0 x 10-3 mmol). The desired nanoparticles were obtained as a light orange solid. (63 mg, 63% recovery). PCS: Z_{ave} (nm) 54.8±2.9; UV/vis: (H^2O) λ (%): 412 (100), 526 (12.4), 563 (5.0)

Nanoconjugates 10. The conjugated nanospecies were obtained following the general procedure, using amino-functionalised nanospecies (70 mg) and porphyrin 6 (4 mg, 3.4 x 10-3 mmol). The desired nanoparticles were obtained as a light orange solid. (60 mg, 70% recovery). PCS: Z_{ave} (nm) 174.3±50.4; UV/vis: (H^2O) λ (%): 403 (100), 527 (10.7), 561 (3.6)

Nanoconjugates 11. The conjugated nanospecies were obtained following the general procedure, using amino-functionalised nanospecies (70 mg) and porphyrin 7 (4 mg, 3.7 x 10-3 mmol). The desired nanoparticles were obtained as a light orange solid. (58 mg, 86% recovery). PCS: Z_{ave} (nm) 59.8±15.5; UV/vis: (H_2O) λ (%): 412 (100), 515 (12.9), 541 (6.9)

Abbreviations

DMF, dimethylformamide; DMSO, dimethylsulfoxide; EDC, 1-ethyl-3-(3-dimethylaminopropyl)carbodiimide; ESI, elec-tron-spray ionisation; MALDI, matrix-assisted laser desorp-tion ionisation; MEM, modified Eagle's medium; MRI, mag-netic resonance imaging; MWI, microwave irradiation; NHS, N-hydroxysuccinimide; NMP, N-methylpyrrolidinone; PBS, phosphate buffered saline; PET, positron emission tomography; TBAC tetrabutylammonium chloride; TFA, trifluoroacetic acid.

Acknowledgements

The authors thank EPSRC for funding the project (EP/H000151/1). Mass spectrometry data was acquired at the EPSRC UK National Mass Spectrometry Facility at Swansea University.

Notes and references

[a] Department of Chemistry, University of Hull, Hull, UK.
[b] School of Pharmacy, University of Nottingham, Nottingham, UK.
[c] Department of Chemistry, University of Durham, Durham, UK.
[d] National Medical Laser Centre, University College London, London, UK.
[d] Institute of Orthopaedics and Musculoskeletal Science, University College London, London, UK.
† School of Pharmacy and Biomolecular Sciences, Liverpool John Moores University, Liverpool, L3 3AF, UK.

Electronic Supplementary Information (ESI) available: [details of any supplementary information available should be included here]. See DOI: 10.1039/b000000x/

1. J. F. Lovell, T. W. B. Liu, J. Chen and G. Zheng, *Chem. Rev.*, 2010, **110**, 2839-2857.
2. J. F. Lovell, A. Roxin, K. K. Ng, Q. Qi, J. D. McMullen, R. S. DaCosta and G. Zheng, *Biomacromolecules*, 2011, **12**, 3115-3118.

3. E. Huynh, J. F. Lovell, B. L. Helfield, M. Jeon, C. Kim, D. E. Goertz, B. C. Wilson and G. Zheng, *JACS*, 2012, **134**, 16464-16467.
4. J. F. Lovell, C. S. Jin, E. Huynh, T. D. MacDonald, W. Cao and G. Zheng, *Angew. Chem. Int. Ed.*, 2012, **51**, 2429-2433.
5. T. Lee, X.-a. Zhang, S. Dhar, H. Faas, S. J. Lippard and A. Jasanoff, *Chemistry & Biology*, 2010, **17**, 665-673.
6. T. W. Liu, T. D. MacDonald, J. Shi, B. C. Wilson and G. Zheng, *Angew. Chem. Int. Ed.*, 2012, **51**, 13128-13131.
7. J. Shi, T. W. B. Liu, J. Chen, D. Green, D. Jaffray, B. C. Wilson, F. Wang and G. Zheng, *Theranostic*, 2011, **1**, 363-370.
8. J. A. Kitchen, R. Parkesh, E. B. Veale and T. Gunnlaugsson, in *Supramol. Chem.*, John Wiley & Sons, Ltd, 2012.
9. D. Papkovsky and T. O'Riordan, *Journal of Fluorescence*, 2005, **15**, 569-584.
10. X. Chen, X. Tian, I. Shin and J. Yoon, *Chem. Soc. Rev.*, 2011, **40**, 4783-4804.
11. Y. Amao, *Microchimica Acta*, 2003, **143**, 1-12.
12. C. O'Donovan, J. Hynes, D. Yashunski and D. B. Papkovsky, *J. Mater. Chem.*, 2005, **15**, 2946-2951.
13. J. Hynes, S. Floyd, A. E. Soini, R. O'Connor and D. B. Papkovsky, *Journal of Biomolecular Screening*, 2003, **8**, 264-272.
14. T. C. O'Riordan, A. E. Soini and D. B. Papkovsky, *Anal. Biochem.*, 2001, **290**, 366-375.
15. T. C. O'Riordan, A. V. Zhdanov, G. V. Ponomarev and D. B. Papkovsky, *Anal. Chem.*, 2007, **79**, 9414-9419.
16. D. B. Papkovsky, G. V. Ponomarev, W. Trettnak and P. O'Leary, *Anal. Chem.*, 1995, **67**, 4112-4117.
17. R. Dmitriev and D. Papkovsky, *Cellular and Molecular Life Sciences*, 2012, **69**, 2025-2039.
18. R. I. Dmitriev, H. M. Ropiak, G. V. Ponomarev, D. V. Yashunsky and D. B. Papkovsky, *Bioconjugate Chem.*, 2011, **22**, 2507-2518.
19. R. I. Dmitriev, H. M. Ropiak, D. V. Yashunsky, G. V. Ponomarev, A. V. Zhdanov and D. B. Papkovsky, *FEBS Journal*, 2010, **277**, 4651-4661.
20. R. I. Dmitriev, A. V. Zhdanov, G. Jasionek and D. B. Papkovsky, *Anal. Chem.*, 2012, **84**, 2930-2938.
21. R. I. Dmitriev, A. V. Zhdanov, G. V. Ponomarev, D. V. Yashunski and D. B. Papkovsky, *Anal. Biochem.*, 2010, **398**, 24-33.
22. K. Koren, R. I. Dmitriev, S. M. Borisov, D. B. Papkovsky and I. Klimant, *ChemBioChem*, 2012, **13**, 1184-1190.
23. I. Dunphy, S. A. Vinogradov and D. F. Wilson, *Anal. Biochem.*, 2002, **310**, 191-198.
24. O. Finikova, A. Galkin, V. Rozhkov, M. Cordero, C. Hägerhäll and S. Vinogradov, *JACS*, 2003, **125**, 4882-4893.
25. A. Y. Lebedev, A. V. Cheprakov, S. Sakadžić, D. A. Boas, D. F. Wilson and S. A. Vinogradov, *ACS Applied Materials & Interfaces*, 2009, **1**, 1292-1304.
26. B. W. Pedersen, L. E. Sinks, T. Breitenbach, N. B. Schack, S. A. Vinogradov and P. R. Ogilby, *Photochem. Photobiol.*, 2011, **87**, 1077-1091.
27. I. B. Rietveld, E. Kim and S. A. Vinogradov, *Tetrahedron*, 2003, **59**, 3821-3831.
28. V. Rozhkov, D. Wilson and S. Vinogradov, *Macromolecules*, 2002, **35**, 1991-1993.
29. C. Wu, B. Bull, K. Christensen and J. McNeill, *Angew. Chem. Int. Ed.*, 2009, **48**, 2741-2745.
30. M. Wacker, K. Chen, A. Preuss, K. Possemeyer, B. Roeder and K. Langer, *Int. J. Pharm.*, 2010, **393**, 254-263.
31. F. Su, R. Alam, Q. Mei, Y. Tian, C. Youngbull, R. H. Johnson and D. R. Meldrum, *PLoS ONE*, 2012, **7**, e33390.
32. A. Fercher, S. M. Borisov, A. V. Zhdanov, I. Klimant and D. B. Papkovsky, *ACS Nano*, 2011, **5**, 5499-5508.
33. Y.-E. Koo Lee, E. E. Ulbrich, G. Kim, H. Hah, C. Strollo, W. Fan, R. Gurjar, S. Koo and R. Kopelman, *Anal. Chem.*, 2010, **82**, 8446-8455.
34. Y.-E. L. Koo, Y. Cao, R. Kopelman, S. M. Koo, M. Brasuel and M. A. Philbert, *Anal. Chem.*, 2004, **76**, 2498-2505.
35. L. E. Sinks, G. P. Robbins, E. Roussakis, T. Troxler, D. A. Hammer and S. A. Vinogradov, *The Journal of Physical Chemistry B*, 2010, **114**, 14373-14382.
36. C.-C. Yang, Y. Tian, A. K. Y. Jen and W.-C. Chen, *J. Polym. Sci., Part A: Polym. Chem.*, 2006, **44**, 5495-5504.
37. H. Xiang, L. Zhou, Y. Feng, J. Cheng, D. Wu and X. Zhou, *Inorg. Chem.*, 2012, **51**, 5208-5212.
38. V. V. Vasil'ev and S. M. Borisov, *Sensors and Actuators B: Chemical*, 2002, **82**, 272-276.
39. V. S. Tripathi, G. Lakshminarayana and M. Nogami, *Sensors and Actuators B: Chemical*, 2010, **147**, 741-747.
40. Y. Tian, B. R. Shumway and D. R. Meldrum, *Chem. Mater.*, 2010, **22**, 2069-2078.
41. Y. Tian, B. R. Shumway, C. A. Youngbull, Y. Li, A. K. Y. Jen, R. H. Johnson and D. R. Meldrum, *Sensors and Actuators B: Chemical*, 2010, **147**, 714-722.
42. S. R. Scheicher, B. Kainz, S. Köstler, M. Suppan, A. Bizzarri, D. Pum, U. B. Sleytr and V. Ribitsch, *Biosens. Bioelectron.*, 2009, **25**, 797-802.
43. M. Obata, N. Matsuura, K. Mitsuo, H. Nagai, K. Asai, M. Harada, S. Hirohara, M. Tanihara and S. Yano, *J. Polym. Sci., Part A: Polym. Chem.*, 2010, **48**, 663-670.
44. K. Koren, S. M. Borisov and I. Klimant, *Sensors and Actuators B: Chemical*, 2012, **169**, 173-181.
45. A. Habibagahi, Y. Mébarki, Y. Sultan and R. J. Crutchley, *Journal of Photochemistry and Photobiology A: Chemistry*, 2011, **225**, 88-94.
46. Y. Amao, T. Miyashita and I. Okura, *J. Fluorine Chem.*, 2001, **107**, 101-106.
47. B. J. Basu, *Sensors and Actuators B: Chemical*, 2007, **123**, 568-577.
48. P. J. Cywinski, A. J. Moro, S. E. Stanca, C. Biskup and G. J. Mohr, *Sensors and Actuators B: Chemical*, 2009, **135**, 472-477.
49. G. DiMarco and M. Lanza, *Sensors and Actuators B: Chemical*, 2000, **63**, 42-48.
50. J. M. Vanderkooi, M. Erecinska and I. A. Silver, *American Journal of Physiology - Cell Physiology*, 1991, **260**, C1131-C1150.
51. H. Suzuki, A. Sugama and N. Kojima, *Sensors and Actuators B: Chemical*, 1993, **10**, 91-98.
52. K. Kellner, G. Liebsch, I. Klimant, O. S. Wolfbeis, T. Blunk, M. B. Schulz and A. Göpferich, *Biotechnol. Bioeng.*, 2002, **80**, 73-83.
53. A. Mishra and B. Starly, *Microfluidics and Nanofluidics*, 2009, **6**, 373-381.
54. S. Sahai, R. McFarland, M. L. Skiles, D. Sullivan, A. Williams and J. O. Blanchette, *Tissue engineering. Part C, Methods*, 2012, **18**, 557-565.
55. V. Soloviev, D. Wilson and S. Vinogradov, *Appl. Opt.*, 2003, **42**, 113-123.
56. V. Y. Soloviev, D. F. Wilson and S. A. Vinogradov, *Appl. Opt.*, 2004, **43**, 564-574.
57. H. C. Harrington, F. R. A. J. Rose, Y. Reinwald, L. D. K. Buttery, A. M. Ghaemmaghami and J. W. Aylott, *Analytical Methods*, 2013.
58. Y. Liu and S. Wang, *Colloids and Surfaces B: Biointerfaces*, 2007, **58**, 8-13.
59. U. Cheema, T. Alekseeva, E. A. Abou-Neel and R. A. Brown, *European Cell Materials*, 2010, **20**, 274-280.
60. U. Cheema, R. A. Brown, B. Alp and A. J. MacRobert, *Cellular and Molecular Life Sciences*, 2008, **65**, 177-186.
61. U. Cheema, E. Hadjipanayi, N. Tammi, B. Alp, V. Mudera and R. A. Brown, *International Journal of Artificial Organs* 2009, **32**, 318-328.
62. I. Streeter and U. Cheema, *Analyst*, 2011, **136**, 4013-4019.
63. L. G. Griffith and M. A. Swartz, *Nat Rev Mol Cell Biol*, 2006, **7**, 211-224.
64. S. M. S. Kazmi, A. J. Salvaggio, A. D. Estrada, M. A. Hemati, N. K. Shaydyuk, E. Roussakis, T. A. Jones, S. A. Vinogradov and A. K. Dunn, *Biomed. Opt. Express*, 2013, **4**, 1061-1073.
65. J. Lecoq, A. Parpaleix, E. Roussakis, M. Ducros, Y. G. Houssen, S. A. Vinogradov and S. Charpak, *Nat Med*, 2011, **17**, 893-898.
66. F. Giuntini, F. Dumoulin, R. Daly, V. Ahsen, E. M. Scanlan, A. S. P. Lavado, J. W. Aylott, G. A. Rosser, A. Beeby and R. W. Boyle, *Nanoscale*, 2012, **4**, 2034-2045.

67. L. B. Josefsen, J. W. Aylott, A. Beeby, P. Warburton, J. P. Boyle, C. Peers and R. W. Boyle, *Photochemical & Photobiological Sciences*, 2010, **9**, 801-811.
68. S. P. Martsev, V. A. Preygerzon, Y. I. Mel'nikova, Z. I. Kravchuk, G. V. Ponomarev, V. E. Lunev and A. P. Savitsky, *Journal of Immunological Methods*, 1995, **186**, 293-304.
69. M. Sirish, V. A. Chertkov and H.-J. Schneider, *Chemistry – A European Journal*, 2002, **8**, 1181-1188.
70. Y. Li, J. Xiao, T. E. Shubina, M. Chen, Z. Shi, M. Schmid, H.-P. Steinrück, J. M. Gottfried and N. Lin, *JACS*, 2012, **134**, 6401-6408.
71. C. M. Drain, A. Varotto and I. Radivojevic, *Chem. Rev.*, 2009, **109**, 1630-1658.
72. H. Krupitsky, Z. Stein, I. Goldberg and C. Strouse, *J. Inclusion Phenom. Mol. Recognit. Chem.*, 1994, **18**, 177-192.
73. S. Lipstman and I. Goldberg, *Crystal Growth & Design*, 2010, **10**, 5001-5006.
74. F. Giuntini, D. Nistri, G. Chiti, L. Fantetti, G. Roncucci and G. Jori, *Tetrahedron Lett.*, 2003, **44**, 515-517.
75. R. F. Pasternack, R. A. Brigandi, M. J. Abrams, A. P. Williams and E. J. Gibbs, *Inorg. Chem.*, 1990, **29**, 4483-4486.
76. S. M. Borisov and I. Klimant, *Dyes and Pigments*, 2009, **83**, 312-316.
77. L. M. Mink, M. L. Neitzel, L. M. Bellomy, R. E. Falvo, R. K. Boggess, B. T. Trainum and P. Yeaman, *Polyhedron*, 1997, **16**, 2809-2817.
78. T. Soller, M. Ringler, M. Wunderlich, T. A. Klar, J. Feldmann, H. P. Josel, J. Koci, Y. Markert, A. Nichtl and K. Kürzinger, *The Journal of Physical Chemistry B*, 2008, **112**, 12824-12826.
79. C. Ringot, N. Saad, R. Granet, P. Bressollier, V. Sol and P. Krausz, *J. Porphyrins Phthalocyanines*, 2010, **14**, 925-931.
80. C. J. P. Monteiro, M. M. Pereira, S. M. A. Pinto, A. V. C. Simões, G. F. F. Sá, L. G. Arnaut, S. J. Formosinho, S. Simões and M. F. Wyatt, *Tetrahedron*, 2008, **64**, 5132-5138.
81. J. D. Moseley and C. O. Kappe, *Green Chemistry*, 2011, **13**, 794-806.
82. M. L. Dean, J. R. Schmink, N. E. Leadbeater and C. Bruckner, *Dalton Transactions*, 2008, 1341-1345.
83. M. Kuruppuarachchi, H. Savoie, A. Lowry, C. Alonso and R. W. Boyle, *Molecular Pharmaceutics*, 2011, **8**, 920-931.
84. D. C. Barber, R. A. Freitag-Beeston and D. G. Whitten, *The Journal of Physical Chemistry*, 1991, **95**, 4074-4086.
85. K. Chen, A. Preuß, S. Hackbarth, M. Wacker, K. Langer and B. Röder, *Journal of Photochemistry and Photobiology B: Biology*, 2009, **96**, 66-74.
86. J. M. Vanderkooi, G. Maniara, T. J. Green and D. F. Wilson, *J. Biol. Chem.*, 1987, **262**, 5476-5482.
87. J. Lakowicz, *Principles of Fluorescence Spectroscopy*, Kluwer Academic/Plenum Publishers, New York, Boston, Dordrecht, London, Moscow, 1999.
88. S. Draxler, M. E. Lippitsch, I. Klimant, H. Kraus and O. S. Wolfbeis, *The Journal of Physical Chemistry*, 1995, **99**, 3162-3167.
89. P. Hartmann, M. J. P. Leiner and M. E. Lippitsch, *Anal. Chem.*, 1995, **67**, 88-93.
90. T. Itoh, K. Yaegashi, T. Kosaka, T. Kinoshita and T. Morimoto, *American Journal of Physiology - Heart and Circulatory Physiology*, 1994, **267**, H2068-H2078.
91. W. L. Rumsey, J. M. Vanderkooi and D. F. Wilson, *Science*, 1988, **241**, 1649-1651.
92. Z. Lin, T. Cherng-Wen, P. Roy and D. Trau, *Lab on a Chip*, 2009, **9**, 257-262.
93. R. H. W. Lam, M.-C. Kim and T. Thorsen, *Anal. Chem.*, 2009, **81**, 5918-5924.
94. U. Cheema, Z. Rong, O. Kirresh, A. J. MacRobert, P. Vadgama and R. A. Brown, *Journal of Tissue Engineering and Regenerative Medicine*, 2012, **6**, 77-84.
95. S. Nonell and S. E. Braslavsky, in *Methods Enzymol.*, ed. H. S. Lester Packer, Academic Press, 2000, pp. 37-49.
96. R. Schmidt, K. Seikel and H. D. Brauer, *The Journal of Physical Chemistry*, 1989, **93**, 4507-4511.
97. D. B. G. Williams and M. Lawton, *J. Org. Chem.*, 2010, **75**, 8351-8354.
98. H. A. Clark, M. Hoyer, M. A. Philbert and R. Kopelman, *Anal. Chem.*, 1999, **71**, 4831-4836.
99. A. Schubert, T. Klütsch and D. Cech, *Nucleosides and Nucleotides*, 1997, **16**, 277-289.
100. J. H. Price, J. P. Birk and B. B. Wayland, *Inorg. Chem.*, 1978, **17**, 2245-2250.